# Numerically Modelling Resonant Cyclotron Scattering in Neutron Stars

Alice Curtin

April 21, 2020

**Abstract**

Neutron stars are a stellar remnant that emit strong thermal radiation from their surface. This radiation is then both absorbed and scattered in the surrounding magnetosphere of the neutron star. In certain cases, the radiation can undergo resonant cyclotron scattering in which the scattering process is unlike inverse Compton or Compton scattering. In this paper, we focus on a specific, one-dimensional model for resonant cyclotron scattering by Lyutikov and Gavriil (2006). We explore the fundamental physics behind resonant cyclotron scattering and then compare our numerical results with those produced by Lyutikov and Gavriil who find that: 1. at high optical depths, a resonant scattering layering is equally opaque to reflections and transmissions and 2. that resonant scattering will up-scatter the initial spectrum. We then discuss the applications of this model to current data and its future usage in neutron star modelling.

## 1 Introduction

When a massive star collapses during a supernovae, one of the possible remnants (dependent on the initial mass of the system) is a neutron star. Neutron stars (NS) are extremely dense objects with small radii that are primarily composed of neutrons (although the equation of state for these objects is still not well constrained). Due to their fairly high surface temperature, around 60,000 K, NS emit strong thermal radiation from their surface. The emitted continuum will then undergo both absorption and scattering in the surrounding medium. We focus on absorption and scattering in the magnetosphere of the NS, a region surrounding the NS consisting of a plasma interacting with the magnetic field lines of the NS. More specifically, we focus on resonant cyclotron scattering. As the electrons in the plasma interact with the magnetic field lines in the magnetosphere, they will produce cyclotron radiation and emit radiation at frequency:

$$\omega_c = \frac{eB}{mc} \tag{1}$$

where $e$ is the charge of the electron, $B$ is the magnetic field strength at the given location of the electron, $m$ is the mass of the electron, and $c$ is the speed of light (all in cgs units). If a photon at the surface of the NS is emitted with the same frequency (or is previously scattered up to that given frequency), the interaction between the electron and the photon takes on a form different than either inverse Compton scattering or Compton scattering (which have both been well studied in the literature).

In particular, for resonant cyclootron scattering to be important, the density of the magnetosphere must be much higher than the Goldreich-Julien density,

$$n_{GR} = \frac{\boldsymbol{B} \cdot \boldsymbol{\Omega}}{2\pi ec} \tag{2}$$

where $\boldsymbol{B}$ is the magnetic field and $\boldsymbol{\Omega}$ is the angular velocity. If $n \approx n_{GR}$, then resonant cyclotron scattering can be ignored, but if $n \gg n_{GR}$, then resonant cyclotron scattering needs to be accounted for. See Ref. [1], section two for more information on the derivation of this lower limit. Possible systems in which $n \gg n_{GR}$ include: 1. certain rotationally powered pulsars, 2. magnetars with large-scale current densities, 3. accreting NS, and 4. certain binary pulsar systems such as PSR J0737-3039B [2].

In this paper, we aim to explore work done by Ref. [2] on numerical modelling of resonant cyclotron scattering in an inhomogenous magnetic field. We start by exploring the underlying parameters (Section 2) and equations for resonant cylcotron scattering (Section 3). In Section 4, we describe the numerical methods necessary to model resonant cyclotron scattering. We then compare our numerical modelling with that performed by Ref. [2] in Section 5. We conclude in Section 6 by describing the application of this model to real data along with ideas for future work related to this topic.

## 2 Resonance Radius, Cross-Section, and Optical Depth

In accordance with Ref. [2], we explore resonant cyclotron scattering in the non-relativistic limit where $T < mc^2/k_B$ where $T$ is the temperature of the region of interest and $k_B$ is the Boltzmann constant. We assume a one-dimensional photon propagation with photons either transmitted or reflected during a given scattering. Additional assumptions made are: 1. the system consists of dipolar magnetic fieds, 2. the plasma is tenuous, 3. the refractive index is $\approx 1$ so Debye screening is ignored, and 4. the radiation is not polarized. It is important to note that the fourth assumption could pose problems as NS surface emission is typically polarized.

The magnetic field of the NS decreases as you move away from the surface, thus the radius at which a photon with energy $\epsilon$ will undergo resonant scattering is:

$$r \sim r_{NS}(\frac{\hbar e B_{NS}}{\epsilon mc})^{1/3} \sim 8 r_{NS} b^{1/3} (\frac{\epsilon}{1\text{keV}})^{-1/3} \tag{3}$$

where $b = B_{NS}/B_c$ with $B_c = 4 \times 10^{13}$ G. For a typical NS, $r_{NS} \sim 10^6$ cm and $B_{NS} \sim 10^{14}$ to $10^{16}$ G. The resonance radius as both a function of the photon energy and the surface magnetic field strength is shown in Fig. 1. As expected from Eq. 1, as the energy of the initial photons increases, the resonance radius decreases. Additionally, as the magnetic field strength increases, the resonance radius for a given photon energy increases.

The radius of resonance, Eq. 3, can be used to define the optical depth of resonance scattering. The optical depth is defined as:

$$\tau_{res} = \int \sigma_{res} n dl \tag{4}$$

where $\sigma_{res}$ is the cross-section of resonance scattering, $n$ is the density, and $dl$ is some infinitesimal length [2]. The cross-section of resonance scattering (derived in its earliest form in Ref. [3]) is given by:

$$\sigma_{res} = \frac{\sigma_T}{4} \frac{(1 + \cos^2 \alpha')\omega^2}{(\omega - \omega_B)^2 \Gamma^2/4} \tag{5}$$

where $\alpha'$ is the angle between the incoming photon and the local magnetic field, $\sigma_T$ is the Thomson cross-section, and $\Gamma$ is the natural line width of the first harmonic of the cyclotron emission given by:

$$\Gamma = \frac{4e^2 w_B^2}{3mc^3}. \tag{6}$$

The natural line width of the first harmonic can be used to determine the transition time for synchrotron emission where $t \sim 1/\Gamma$. For photons to be emitted and not purely absorbed, $t < r/c$ where $r/c$ is the dynamical time of the system. This occurs if $r < 7.6 \times 10^8 b^{2/5}$ cm which is equivalent to an energy of $\epsilon > 10^{-3} b^{-1/5}$ eV [2]. Thus, resonance cyclotron scattering is most relevant for higher energy photons such as x-ray or gamma-ray photons as lower energy radiation is typically absorbed rather than scattered.

We can now insert Eq. 5 into Eq. 4 to get:

$$\tau_{res} = \tau_0 (1 + \cos^2 \alpha') \tag{7}$$

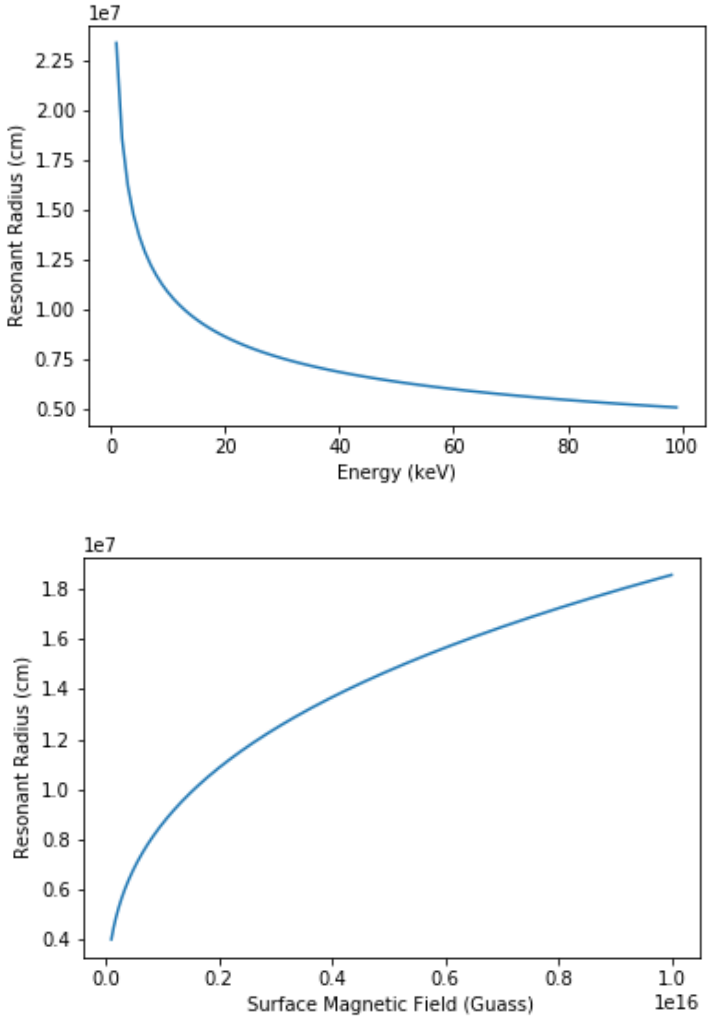


Figure 1: Resonance radius as a function of both initial photon energy and neutron star surface magnetic field strength for a neutron star with $r_{NS} = 10^6$ cm.

where $e^{-\tau_0}$ is the number of photons that are not scattered in this space and $\tau_0$ is given by:

$$\tau_0 = \frac{\pi^2 e^2 n r}{3mc\omega_B}. \tag{8}$$

Assuming a one-dimensional photon propagation, $\alpha'$ is equal to either 0 or $\pi$ such that:

$$\tau_{res} = 2\tau_0. \tag{9}$$

The resonance cross-section as a function of frequency for a given photon energy is shown in Fig. 2. While Fig. 2 does not present any new information, it does confirm that the relation between $r$, $B_{NS}$, $\omega_B$, and $\sigma_{res}$ since the magnitude of the cross-section peaks at the frequency corresponding to the initial energy of the photon. If any of the fundamental relations are changed between $r$, $B_{NS}$, etc., Fig. 2 does not peak at the correct frequency.

Assuming the same relation as Eq. 4 for Thomson scattering with $\sigma_{res}$ replaced by $\sigma_T$, we can derive a ratio between the two optical depths:

$$\frac{\tau_{res}}{\tau_T} = \frac{\pi}{8}\frac{c}{r_e\omega_B} \tag{10}$$

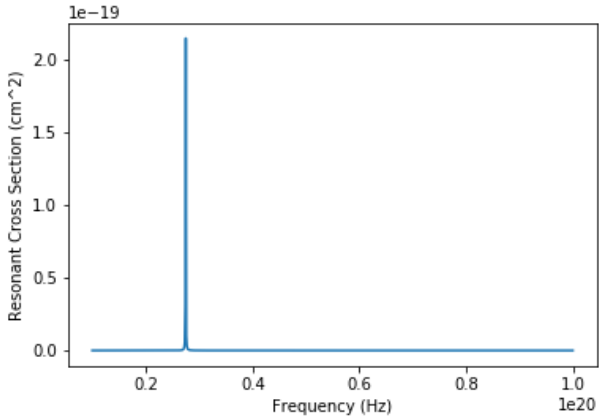


Figure 2: Resonant cross-section as a function of frequency for an initial magnetic field strength of $10^{12}$ G, a neutron star radius of $10^6$ cm, and a photon energy of 20 keV.

where $r_e$ is the classical radius of an electron [2]. As seen in Fig. 3, the resonant cross-section can be four orders of magnitude larger than the Thomson cross-section for x-ray photon energies and for higher energy photons, resonant cyclotron scattering cannot be ignored.

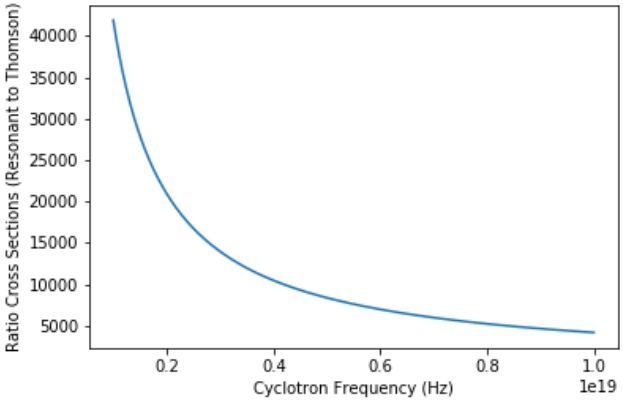


Figure 3: Ratio of the resonant cyclotron scattering cross-section to the Thomson cross-section for x-ray frequencies.

## 3 Derivation of Transfer Equations

In order to model resonant cyclotron scattering, we follow the methods outlined by Ref. [2], herein referred to as Lyutikov and Gavriil. The key equations are based off of the radiative transfer equations for line-driven winds. While each step of the derivation is not shown here (see Ref. [2]), the general process along with the key equations are described below.

The general equation that needs to be solved is the photon transfer equation:

$$k^\mu \partial_\mu n = \int S f_e \frac{d^3p}{\gamma} \tag{11}$$

where $k^\mu$ is the 4-momentum, $n$ is the photon occupation number, $f$ is the distribution function for electrons, $S$ is the collision rate between photons with occupation number $n$ and distribution function $f$, and $\int d^3p$ is an integral over momentum space. Because we are in the non-relativistic limit, we are only concerned with terms that are linear in $\beta$ where $\beta = v/c$. To solve Eq. 11,

Lyutikov and Gavriil transform first to the electron's frame of rest, and then the frame of the plasma where they introduce the invariant collision integral. They neglect all recoil terms, as these are higher order in $\beta$, and transform back to the laboratory frame. They then impose the conditions of a one-dimensional, non-relativistic electron distribution in a stationary plasma. They apply the Schwarzchild-Schuster method in which the initial radiation field is assumed to be isotropic such that the intensity integral (or in this case the source function integral) is broken up into a sum for photons propagating in the forward and backward direction. Thus, the Schwarzchild-Schuster method simplifies the complex system into a one-dimensional system.

Next, Lyutikov and Gavriil impose the conditions of an inhomogenous magnetic field in which both the magnitude and direction of the field vary. These effects are the most important in the magnetosphere of the system where the width of the spatial resonance, $\Delta r$, is much smaller than the scattering layer thickness, $H$, where we assumed the scattering layers are plane parallel slabs. In the photosphere of the NS, cyclotron resonant scattering might still occur, but in this region $\Delta r > H$. Thus, after one scatter, the photon will likely no longer lie within the scattering layer, and will leave the regime of resonance scattering. For an initially continuous spectrum, this will take the form of an absorption line at the resonance frequency. However, if $\Delta r < H$, then the photons can be continuously scattered, transforming the entire initial spectrum.

In an inhomogenous medium, we need to account for the photon's movement through the scattering layer (real space) and their doppler shifts (frequency space). Lyutikov and Gavriil transform variables to a system in which the conserved quantity becomes the velocity of the electron, $\beta$, rather than $\omega$ in order to easily account for both frequency and space changes. Additionally, Lyutikov and Gavriil assume a constant density for the magnetosphere such that the optical depth is a function of only $\beta$. They assume a water bag distribution of particles with:

$$\tau(\beta) = \begin{cases} \frac{\tau_0}{2\beta_T} & |\beta| < \beta_T \\ 0 & \text{anything else} \end{cases} \tag{12}$$

where $\beta_T$ is the thermal velocity of the electrons. This greatly simplifies the analytical modelling. Applying the initial condition that the photon wave falls only on the inner boundary of the resonant layer and using a Green's function to solve the differential equation, Lyutikov and Gavriil derive the final equations for transmitted and reflected fluxes (shown in Eq. 36 of Ref. [2]). While the result is rather complex, it simplifies in the limit of both large and small optical depths. For small optical depths, the transmitted flux is given by:

$$n_+ = \delta(\omega - \omega_0)(1 - \frac{\tau_0}{4\beta_T}(\omega - \omega_0(1 - 2\beta_T))) \tag{13}$$

while the reflected flux is given by:

$$n_- = \frac{\tau_0}{4\beta_T} \tag{14}$$

where $\omega_0$ is the initial frequency of the light entering into the resonance region centered at $\omega = \omega_0$. For large optical depths, Eq. 13 becomes:

$$n_+ = \frac{\sqrt{\tau_0/\beta_T}}{4\sqrt{2\pi}\omega_0}(1 + 4\beta_T - \frac{\omega}{\omega_0})^{1/4}(\frac{\omega}{\omega_0} - 1)^{-3/4} e^{-(\omega - \omega_0(1+2\beta_T))^2 \tau_0/(16\beta_T^2\omega_0^2)} \tag{15}$$

while Eq. 14 becomes:

$$n_- = \frac{\sqrt{\tau_0/\beta_T}}{4\sqrt{2\pi}\omega_0}((1 + 2\beta_T - \frac{\omega}{\omega_0})(\frac{\omega}{\omega_0} - 1 + 2\beta_T))^{-1/4} e^{-(\omega - \omega_0)^2 \tau_0/(16\beta_T^2\omega_0^2)}. \tag{16}$$

# 4 Numerical Modelling

Eqs. 13, 14, 15, and 16 are reproduced and shown in Fig. 4 and Fig. 5. In order to obtain the correct behaviour of exponential decay as $\omega$ becomes much larger than $\omega_0$, additional negative signs are included in the exponential functions for Eq. 13 and Eq. 15 that were not originally

included in Lyutikov and Gavriil. Additionally, a factor of $\omega_0$ is removed from the denominator of Eq. 13 and Eq. 15 as $\tau_0$ and $\beta_T$ are on the order of 1 while $\omega_0$ is on the order of $10^{18}$ to $10^{20}$.

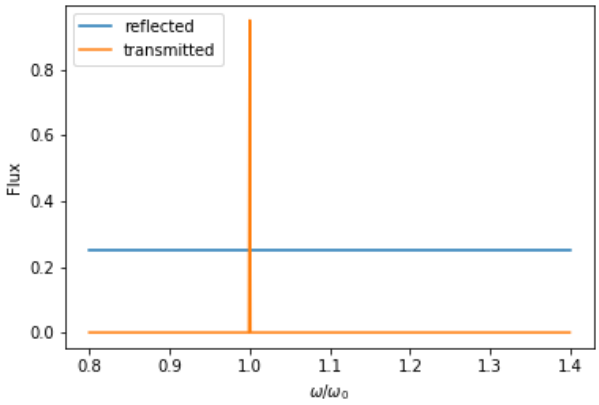


Figure 4: Flux as a function of frequency ratio for a small optical depth of $\tau_0 = 0.1$. The initial magnetic field strength in the magnetosphere is $10^{12}$ G which corresponds to an initial frequency $\omega_0$ of $1.7 \times 10^{19}$ Hz. We assume $\beta_T = 0.1$.

Assuming $\Delta r < H$ such that the resonant scattering width is much smaller than the scattering layer, a given photon can pass through multiple resonant layers. Thus, a photon can be reflected multiple times before finally being transmitted through the scattering layer. In order to model this, we start with an initial Planck function for the radiation from the surface of the NS. We then sum over different reflection possibilities (no reflections, reflecting once then transmitting, reflecting twice then transmitting, etc). such that the observed spectrum becomes:

$$n_{obs} = \int n_s(\omega_0) n_+(\omega, \omega_0) d\omega_0 + \int n_+(\omega, \omega_1) d\omega_1 \int n_s(\omega_0) n_-(\omega_1, \omega_0) d\omega_0 + ..... \tag{17}$$

where $n_s(\omega_0)$ is the value of the initial spectrum at a particular frequency $\omega_0$, $n_+(\omega, \omega_0)$ is a transmission that takes a photon from frequency $\omega_0$ to frequency $\omega$, and $n_-(\omega_1, \omega_0)$ is reflection that takes a photon from frequency $\omega_0$ to frequency $\omega_1$.

## 5 Comparison of Numerical Results with Lyutikov and Gavriil

Our work was aimed at replicating that of Lyutikov and Gavriil (2006). As a result, we directly compare Figs. 4 and 5 with Fig. 6 which is taken from Lyutikov and Gavriil. While we examine slightly different $\tau_0$ examples, the scales and trends of our figures are in agreement with those created by Lyutikov and Gavriil.

At small optical depths, photons are only transmitted at the resonant frequency while the reflected photon distribution is approximately constant and proportional to $\tau_0$. At much larger optical depths, an equal number of photons are transmitted and reflected. This is different than the case of non-resonant scattering and resonant scattering in a homogeneous magnetic field. The reflected photons are centered at $\omega_0$ while the transmitted photons are up-scattered in frequency and energy space by approximately $1 + 2\beta_T$ as a result of the inhomogeneous magnetic field [2]. As can be seen in Fig. 5, the peak flux for the transmitted wave occurs at a slightly lower frequency ratio for $\tau_0 = 10$ than for $\tau_0 = 20$. Additionally, for $\tau_0 = 10$, the transmitted distribution tends away from a distribution to a delta function at $\omega/\omega_0 = 1$. Also, as $\tau$ increases, the width of the reflected and transmitted distributions decreases. This is again in contrast to non-resonant scattering where the dispersion increases as $\tau$ increases. For further derivation of the opaque nature at large optical depths along with the up-scatter in energy, see section 3.3 of Lyutikov and Gavriil.

We also explore the effect that resonant cyclotron scattering has on an initial Planck spectrum, shown in Fig. 7. While Eq. 17 contains an infinite number of terms, Lyutikov and Gavriil note that it converges to within an error of two percent for only six terms. In our calculations, we limit our work to the first term in Eq. 17. As shown in Fig. 7, for $\tau_0 \ll 0$, the final spectrum is very

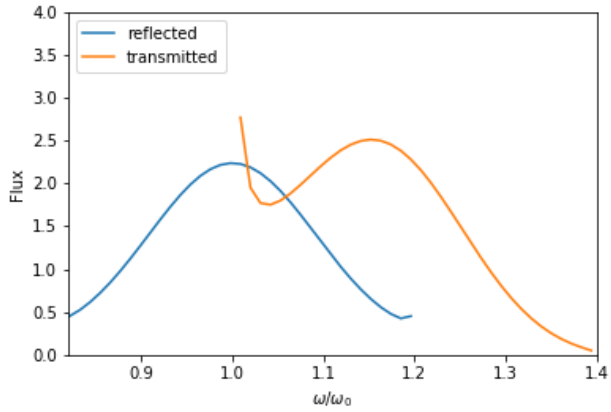


(a) $\tau_0 = 10$

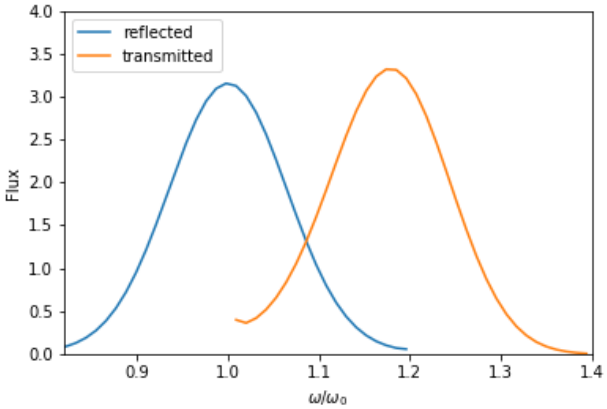


(b) $\tau_0 = 20$

Figure 5: Flux as a function of frequency ratio for two large optical depths. The initial magnetic field strength in the magnetosphere is $10^{12}$ G which corresponds to an initial frequency $\omega_0$ of $1.7 \times 10^{19}$ Hz. We assume $\beta_T = 0.1$.

similar to the initial Planck spectrum as expected since there is little scattering of the photons. For $\tau_0 > 0$, the spectrum remains Planckian with a smaller intensity as more photons are reflected (see the upper right image of Fig. 6). For large optical depths, the entire spectrum is shifted up in both energy and intensity. We do not model the region between $10 > \tau_0 > 0.5$ as this region is $\sim 1$ and thus cannot be described by Eqs. 13, 14, 15, or 16.

We compare our results, Fig. 7, to those of Lyutikov and Gavriil, Fig. 8. For both small and large optical depths, the spectrum in Fig. 8 remains Planckian although the entire distribution is shifted to the right. This is less apparent for $\tau_0 = 0.5$ and most apparent for $\tau_0 = 10$ where the distribution is again shifted by by $1 + 2\beta_T$. Note there is slightly discrepancy betweeen our $\tau_0 = 10$ case and that produced by Lyutikov and Gavriil. This discrepancy, however, can likely be attributed to the limited number of terms we use in our simulation.

For $\tau_0$ on the order of 1, the spectrum produced by Lyutikov and Gavriil is no longer Planckian. As shown in the upper right image of Fig. 6, the reflected flux greatly increases for $\tau_0 \sim 1$ such that the distribution is similar to the initial photon distribution. However, unlike $\tau_0 = 0.1$, the reflected spectrum remains highly dispersed throughout the frequency ratio. As $\tau$ continues to increase, this dispersion decreases. Thus, $\tau_0 \sim$ a few is a special case in-between the two extremes of low and high optical depth that results in a non-Planckian final spectrum.

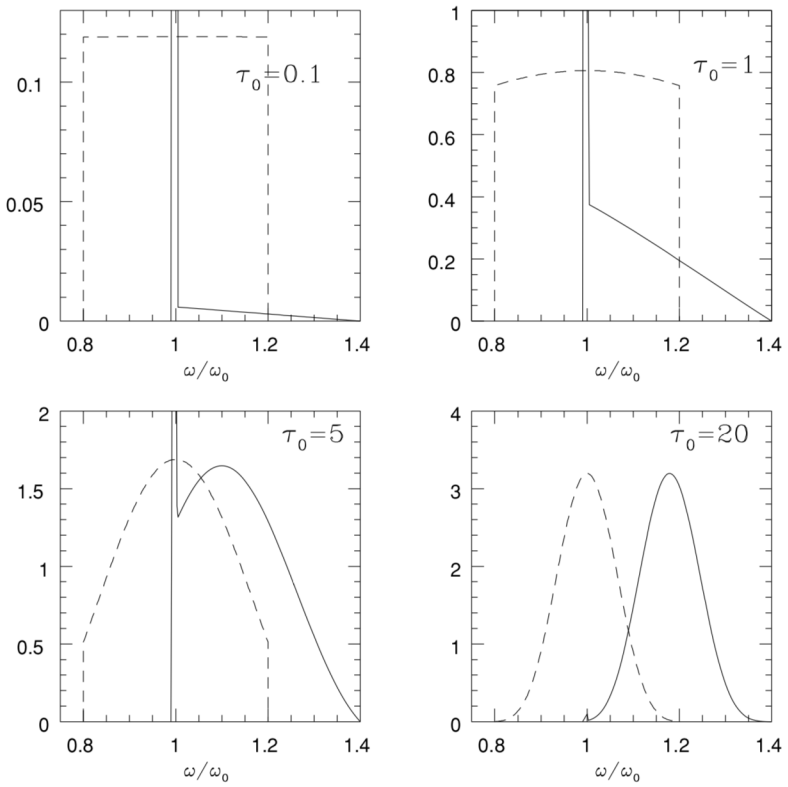


Figure 6: Flux as a function of frequency ratio for both small and large optical depths with $\beta_T = 0.1$. Solid lines correspond to transmitted photons while dashed lines correspond to reflected photons. Image courtesy of Ref. [2].

# 6 Applications and Future Work

Lyutikov and Gavriil applied their model to the x-ray pulsar 1E 1048.1-5937. X-ray pulsars such as this one are usually modelled using both a blackbody and a power law. However, while these two models fit nicely together, it is difficult to justify why both would be necessary. The advantage to the model developed by Lyutikov and Gavrii is that it is a single-component model with a clear process responsible for its result. Additionally, low energy cut-offs are normally needed in blackbody plus power law models while there is a natural cut-off in the resonant cyclotron scattering model as low energy photons will not resonant scatter. In fitting their model to the data, Lyutikov and Gavriil fixed both $\beta_T$ and $\tau_{res}$ and freely varied the temperature, normalization, and hydrogen column density for the pulsar. They then varied both $\beta_T$ and $\tau_{res}$ until they minimized $\chi^2$, with a final $\chi^2$ of 1.05. They found that their model fit the data just as well as the blackbody plus power law combination.

A slightly later version of Lyutikov and Gavriil's model (see Ref. [4]) was developed into code that can now be applied to x-ray data using XSPEC, a part of the NASA's HEASARC software. The model consists of three free parameters: $T$, the temperature of the blackbody seed photons, $\tau_{res}$, and $\beta_T$. A number of sources have since used this model to fit x-ray data from both magnetars (see Ref. [5]) and pulsars (see Ref. [4]).

The temperature fit to Lyutikov and Gavriil's model is different than that fit using the blackbody plus power law. If a continuum of photons underwent resonant cyclotron scattering, their observed temperature would be higher than the intrinsic temperature, as the entire spectrum is shifted upwards in energy. This would, in turn, affect the derived NS radius which is a crucial component in determining the equation of state for NS.

This work might additionally affect the spectral line features of NS. It is expected that the atmospheres surrounding the NS would produce spectral lines, but these features are not commonly observed. Lyutikov and Gavriil ran a simulation in which a spectrum with an emission line underwent resonant cyclotron scattering. While the emission line was prominent in the initial

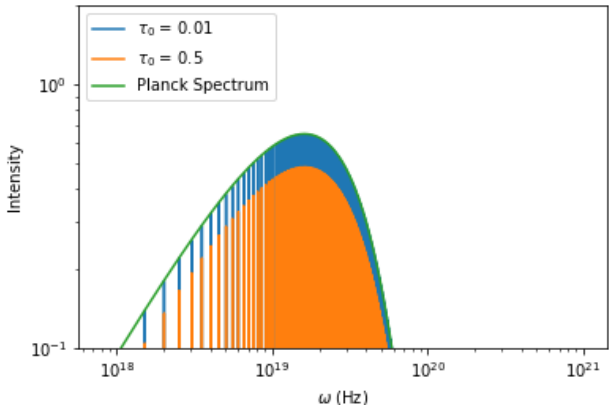


(a) $\tau_0 \ll 0$

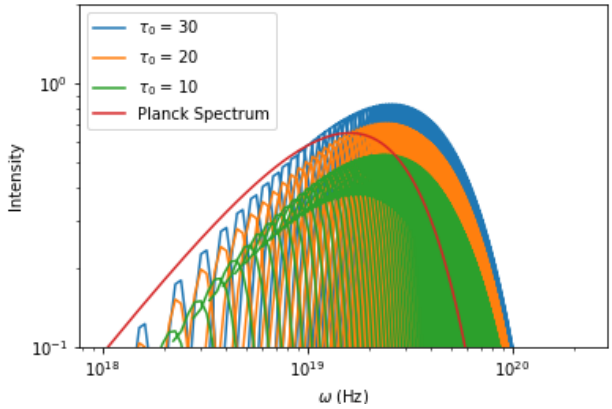


(b) $\tau_0 \gg 0$

Figure 7: Transmitted spectrum as a function of frequency for an initially Planckian spectrum with $\beta_T = 0.3$, $B = 10^{12}$ G and $r_{NS} = 10^6$ cm. Frequencies range from approximately $10^{18}$ Hz to $10^{20}$ Hz. Only one transmission is included in the above plots (no reflections).

Planck spectrum, they found that resonant cyclotron scattering greatly diminished the emission feature, making it difficult to observe. This can also be seen in 3D simulations done by Fernandez and Thompson [6].

Since the work done by Lyutikov and Gavriil, 3D Monte Carlo simulations have been performed by Ref. [6]. While Ref. [6] did not test their model against data, they explored a 3D Monte Carlo simulation of resonant cyclotron scattering with focus on its application to anomalous X-ray pulsars and soft gamma repeaters. While their model was able to reproduce the simulated anomalous X-ray pulsar spectra, it could not account for part of the soft gamma repeater spectra. On the other hand, Ref. [7] created another 3D Monte Carlo simulation of resonant cyclotron scattering with the goal of comparing it to the soft x-ray emission of soft gamma-ray repeaters and x-ray pulsars. When fitting their model against data from CXOU J1647−4552, they were able to find a fit with a $\chi^2$ of 0.81, providing strong support for the usage of either this or similar models in future magnetar and pulsar modelling.

Future work is needed to determine the role of resonant scattering in pulsars, soft gamma repeaters, and magnetars. While this field has continued to grow, there is still the possibility for future refinement of resonant cyclotron models, along with additional testing of it against both old and future observational data. Hopefully this model can then begin to shed more light on the fundamental mechanisms behind the spectra of neutron stars and their equation of state.

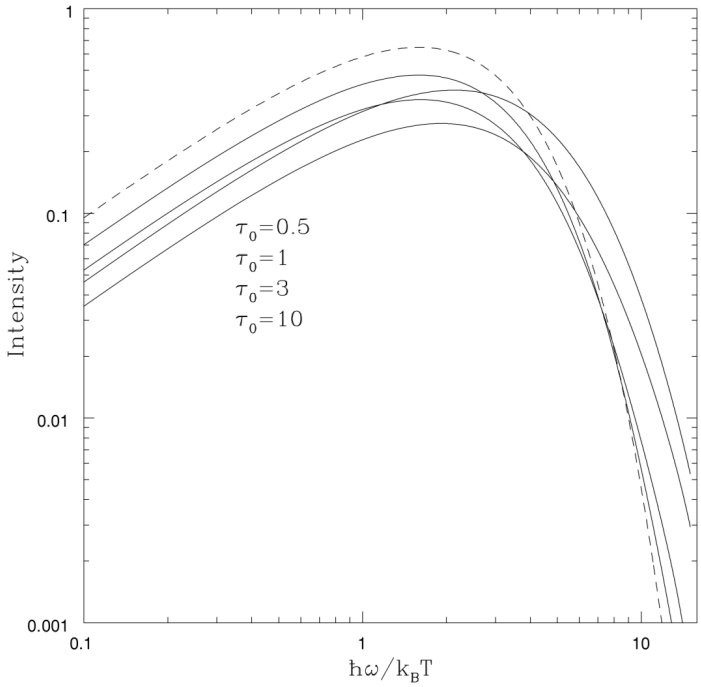


Figure 8: Transmitted spectrum as a function of frequency for an initially Planckian spectrum with $\beta_T = 0.3$. Six different reflection and transmission combinations are included for the above results. The dashed line corresponds to the initial Planck spectra. The curve corresponding to $\tau_0 = 1$ is second from the bottom for the x-coordinate 0.1. Image courtesy of Ref. [2].

# References


[1] A. Mikhailovskii, O. Onishchenko, G. Suramlishvili and S. Sharapov, *The Emergence of Electromagnetic Waves from Pulsar Magnetospheres*, Soviet Astronomy Letters **8** (1982), pp. 685–688

[2] M. Lyutikov1 and F. P. Gavriil, *Resonant cyclotron scattering and Comptonization in neutron star magnetospheres*, MNRAS **368**

[3] A. K. Harding and J. Daugherty, *Cyclotron resonant scattering and absorption*, APJ **374** (1991), pp. 687–699

[4] N. Rea, S. Zane, M. Lyutikov and R. Turolla, *Our distorted view of magnetars: application of the Resonant Cyclotron Scattering model*, Astrophys. Space Sci **308** (2007), pp. 61–65

[5] N. Rea, S. Zane, R. Turolla, M. Lyutikov and D. Gotz, *Resonant cyclotron scattering in magnetars' emission*, APJ **686** (2008)

[6] R. Fernández and C. Thompson, *Resonant Cyclotron Scattering in Three Dimensions and the Quiescent Non-thermal X-ray Emission of Magnetars*, APJ **660** (2006), pp. 615–640

[7] L. Nobili, R. Turolla and S. Zane, *X-ray spectra from magnetar candidates – I. Monte Carlo simulations in the non-relativistic regime*, Monthly Notices **386** (2008), p. 1527–1542